Journal of Applied Electrochemistry
https://doi.org/10.1007/s10800-022-01669-y

RESEARCH ARTICLE

A novel of 2D-3D combination carbon electrode to improve yeast microbial fuel cell performance

Marcelinus Christwardana[1] · **J. Joelianingsih**[1] · **Linda Aliffia Yoshi**[1]

Received: 9 August 2021 / Accepted: 1 January 2022

Abstract

This study developed a unique and outstanding 2D-3D anode using an Activated Carbon (AC) or Charcoal Powder (CP) coating on the carbon felt (CF) surface. The anode structure's high surface area and outstanding electrical conductivity were discovered to improve the enrichment and growth of yeast (*Saccharomyces cerevisiae*) and promote extracellular electron transfer (EET) from the yeast to the anode surface in a Microbial Fuel Cell (MFC) system. Subsequently, an extensive characterization including surface morphology, X-ray diffraction, electrochemical analysis, and biofilm adhesion tests, was performed to the hybrid material's suitability as an MFC anode. The maximum power density of an MFC, installed with the CF/AC as a 2D-3D hybrid anode, was 54.58 mW m^{-2} or 442% higher, compared to the bare CF counterpart. In addition, the hybrid anode produced an internal resistance of 345 Ω in the MFC or about 77% lower, compared to the bare CF counterpart. This improved performance was in turn responsible for the 2.26-fold increase in the quantity of biofilm deposited at the CF/AC anode surface, compared to the bare CF counterpart. Therefore, this hybrid anode manufactured using a simple dip-coating method is a promising anode for high-performance MFC applications.

Graphical abstract

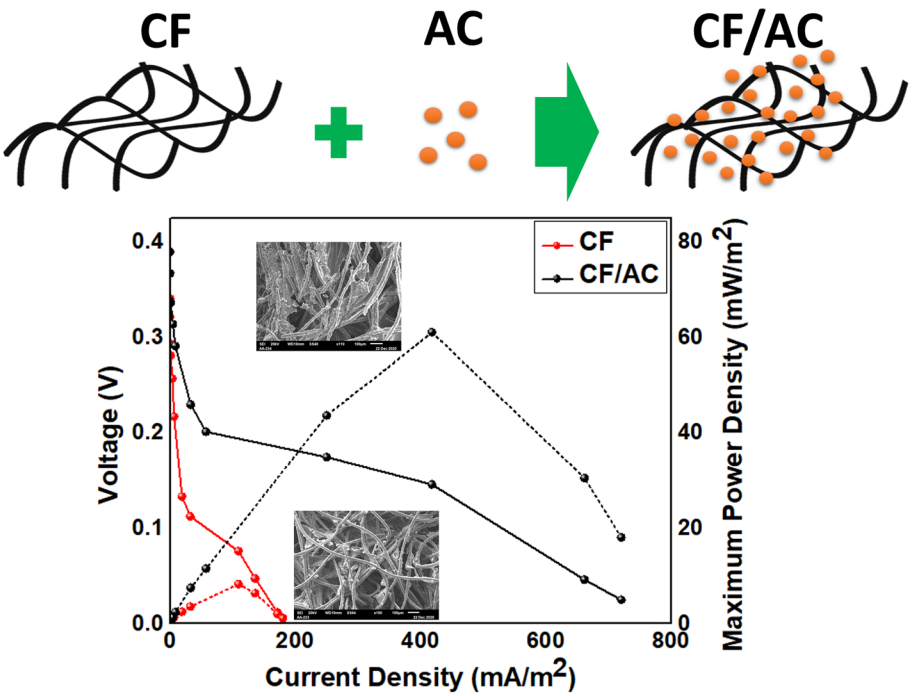

Keywords Hybrid carbon electrode · Dip coating process · Porous electrode · Surface area · Biofilm adhesion

Extended author information available on the last page of the article

Published online: 11 January 2022

1 Introduction

Microbial fuel cells (MFCs) are electrical instruments with the ability to convert the chemical energy in certain substrates into electricity, using microbes as biocatalysts. An MFC has special characteristics, including room-temperature operation, relative ease of use, and high selectivity of the microbes used [1, 2]. Therefore, these cells have the potential to function as a novel technology to remove organic matter during waste treatment processes and an indicator in applications of environmental biosensors [3]. However, MFCs also have significant technological limitations for practical applications, including relatively low power output and efficiency, slow electron transfer, and poor long-term stability, compared to conventional fuel cells; therefore, solutions are required to combat these challenges [4, 5].

Numerous factors influence an MFC's performance, including the cell's anode, architecture, and membrane separation. The anode not only works as supportive material for the growth and development of active bacteria but also accumulates electrons released by bacterial exoelectrogens and, therefore, has the most significant influence on the cell's performance. Several approaches have been attempted to improve the MFC anode's material and composition, to enable the transfer of bacterial adhesion and extracellular electron (EET) from bacteria to the anode.

Furthermore, numerous conventional 2D or 3D carbon-based materials, including activated carbon, carbon brushes, carbon/graphite felt, carbon rods, and carbon cloth/paper have been used as MFC anodes [6–8], due to several benefits, for instance, high flexibility, strong electrical conductivity, and corrosion resistance [9]. However, the use of 2D or 3D electrodes alone is not effective to improve MFC performance due to several inherent problems, including the relatively complicated re-stacking procedure, low ion conductivity, relatively poor stability, and complex manufacturing [10]. The synthesis of a 2D-3D carbon is, therefore, an excellent step, as the hybrid electrode is supposed to have certain benefits, for instance, a larger surface area, open transport ion channels, and all electrode surfaces are ion-moving, compatible with flexible devices, easier to coat, as well as possess larger volumetric storage properties. Based on numerous references, a carbon hybrid electrode comprises two or more carbon allotropes and typically has improved mechanical as well as electrical properties [11, 12]. However, in the production of a 2D-3D carbon hybrid, the smooth linking of these two architectures is often challenging [13, 14]. Furthermore, the application of these hybrid structures, particularly for MFCs, has rarely been studied.

Activated carbon (AC) is highly porous 2D carbon with a broad surface, large electrocatalytic activity and is commonly used as a low-cost substitute for noble metal electrodes in MFCs or conventional fuel cells [15–17]. However, AC is a less common substitute for the anode, due to low electric conductivity [18]. Meanwhile, carbon felt (CF) as 3D carbon, is generally used as an electrode due to the suitable electronic conduction, high surface area, and porosity, thus, providing abundant redox reaction sites, excellent electrolytic strength, mechanical stability, and relatively low cost [19–22]. Therefore, in the manufacture of a 2D-3D hybrid electrode, CF's benefits overcome the weaknesses of AC, and an excellent electrode is obtained. The hybrid electrode's high electrical conductivity is likely to promote EET, while the large surface area is bound to enhance bacterial adherence and enrichment [23].

Several investigations on the modification of carbon/graphite felt with several other materials have been conducted. Shi et al., [24] modified carbon felt with ZnO and activated carbon for zinc-nickel battery applications. Shahzeydi et al. [25] modified copper nanoparticles in carbon felt for catalytic applications. Meanwhile, Ganiyu et al. [26] adapted CoFe-layered double hydroxide on carbon felt for the heterogeneous electro-Fenton process. Shen et al. [27] modified TiO2 monoliths on carbon felt for photocatalytic methyl orange degradation. Based on the existing state of the art of modified carbon felt, modification of carbon felt utilizing activated carbon or charcoal powder for yeast MFCs applications without binder addition (binderless) has never been done previously. As a result, we claim this as an academic novelty in our study.

In this study, a carbon felt anode was coated with activated carbon or charcoal powder (CP) through a dip process, to form a 2D-3D hybrid anode, and the MFC's performance was represented by the voltage value and polarization curves of the CF Anode, modified using AC or CP. In addition, scanning electron microscopy (SEM) and X-ray diffraction (XRD) analyses were performed to evaluate the formation of biofilms on the anode's surface and define the hybrid structure's crystallography characteristics, respectively.

2 Materials and methods

2.1 Carbon felt-based electrode modification

The carbon felt (CF) electrode based on polyacrylonitrile (PAN) was obtained from KWK Steel Co., Ltd (Zhejiang, China) and sliced into circular pieces of 3.5 cm in diameter (7 cm^2 area), as well as 1 cm thickness. Subsequently, the electrode was immediately soaked in 1 M NaOH (Sigma Aldrich, St. Louis, USA) and boiled for 1 h to hydrophilicate the fibers [15]. These hydrophilic fibers help encourage the entry of electrolyte elements containing substrates and

microbes, into the electrode's innermost parts, thus, maximizing the biocatalytic mechanism and substrate degradation. The CF was then washed with deionized water to obtain a pH of 7, and dried at 70 °C, before use. Figure 1 shows the CF's hydrophilicity, where the water forms an angle of 110° on the untreated CF surface but is fully absorbed after treatment with NaOH. This change from hydrophobicity to hydrophilicity also influences the reduction in resistivity from 4717 ± 538 to 1444 ± 298 Ω-cm.

Subsequently, the 2D-3D electrode fabrication process was performed using the method described by Zhang et al., [28]. Activated carbon (AC) powders PRA-A5005AEX were obtained from Panasonic (Osaka, Japan), dispersed in distilled water at a concentration of 5 mg/mL, and then sonicated for 1 h to exfoliate impurities from the powder pores. The dispersion was then washed to eliminate impurities and diluted to a concentration of 1 mg/mL, and then the treated carbon felt was immersed in the AC solution for 2 h, without any binder addition. This was followed by separating the electrode from the solution, washing with distilled water to remove unbound AC, and drying at 70 °C, to become CF/AC. Meanwhile, a combination of carbon felt and charcoal powder (CP), obtained from the local market in Serpong (South Tangerang, Indonesia) was used to produce CF/CP, following the same process.

2.2 Electrochemical measurement

A single-chamber MFC reactor made of acrylic was purchased from Phychemi Co. Ltd. (Beijing, China), and the anode chamber was been filled with an anolyte of 28 mL of fresh YPD medium, composed of 5 mg mL^{-1} of yeast extract (Merck, Darmstadt, Germany), 2.5 mg mL^{-1} of peptone (Himedia, Mumbai, India), 14 mg mL^{-1} of D-glucose (Merck, Darmstadt, Germany), and 14 mg/mL of baker yeast *Saccharomyces cerevisiae* (Lessafre, Marcq-en-Baroeul, France) as a biocatalyst [29–31]. In this case, glucose served as the fuel, with yeast extract functioning as an artificial mediator [32] and peptone acting as a supplement for yeast growth [33]. The cathode was plain CF that was exposed to ambient air directly, while treated Nafion 117 (treated with 3% w/w H_2O_2, 0.5 M H_2SO_4, and DI water) was used as a membrane separator, and modified CF served as the anode. Subsequently, the electrodes were placed in the necessary compartments, and the experiments were conducted at room temperature of about 25 °C, using a conductive stainless-steel wire as the current collector.

The effectiveness of the 2D-3D carbon felt-based anodes was analyzed based on the parameters of the output voltage and power density. In addition, the MFC reactor was paired with the UNI-T UT61E multimeter (Dongguan, China) and supplied with an external load of 1000 Ω for voltage determination. Meanwhile, a data acquisition system controlled the output voltage for 144 h every 15 min, and fresh media were injected every 48 h. Also, loads of 5 MΩ – 10 Ω (Elenco RS500 Resistance Substitution Box, Illinois, USA) were attached between the anode and cathode for the MFC discharge to calculate the power density, while a data acquisition system tracked the output voltage for 30 min, in each 10-min cycle. Subsequently, the current density (J) and maximum power density (MPD) were calculated based on Eqs. (1) and (2), as shown in the following equation:

$$J = \frac{V}{R \times A}, \tag{1}$$

$$MPD = J \times V, \tag{2}$$

where V indicates the voltage (V) between the anode and the cathode, R represents the external resistance (Ω), and A signifies the anode surface area (m^2). Each measurement was repeated at least thrice, and the results were presented as the average value and standard deviation.

2.3 Contact angle, XRD, SEM, and biofilm characterization

The images for contact angle analysis were obtained perpendicular to the corresponding sample surface with a Nikon D5100 DSLR camera (Tokyo, Japan), and angle measurements were done manually with a protractor. The crystalline morphology of the modified CF anodes was determined using X-ray diffractions Rigaku SmartLab SE (Tokyo, Japan) operated at 40 kV, 30 mA, and 5–80° (2θ), with CuKα as the radiation (λ = 1.5406 nm). Meanwhile, scanning electron microscopy FEI Inspect F50 (Oregon,

Fig. 1 The contact angle between water and untreated CF as well as CF treated with NaOH

USA) was used to observe the modified CF anodes' surfaces. The resistance of the modified CF anode was then calculated using the four-point sample method [34], while the yeast biofilm was measured by subtracting the anode's weight before incubation from the weight after incubation.

2.4 Anode surface area determination

The anode's surface area serves as a confirmation of the increase of surface area after modification with CP or AC, and must, therefore, be measured. In this study, the anode surface area was determined using the equation by Maltsev et al., [35] based on reduction in the absorbance of methylene blue, due to absorption by carbon-based electrodes, as shown in Eq. (3):

$$S\left(\frac{m^2}{g}\right) = \frac{1.994\left([MB]_{init} - [MB]_{fin}\right)M_{sol}}{m_c}, \quad (3)$$

where S represents the surface area, $[MB]_{init}$ and $[MB]_{fin}$ indicate the initial and final methylene blue concentrations, respectively, M_{sol} denotes the solution's weight, and m_c signifies the weight of the carbon-based electrode.

2.5 Particle size determination and porosity analysis

Particle size and distribution were measured using Gilson Tapping 8in Sieve Shaker SS-8R (Ohio, USA) with a size of 100 – 635 mesh. Meanwhile, porosity is measured based on bulk and particle density using Eq. (4):

$$\text{Porosity}(\%) = \left(1 - \frac{\text{Bulk density}}{\text{Particle density}}\right) \times 100\%. \quad (4)$$

3 Results and discussion

3.1 Characterization of CP and AC

This is critical for characterizing the CP and AC that will be utilized to modify the CF. As a response, the porosity, particle size distribution, and pH of CP and AC were investigated. The porosities of CP and AC were 22.15 and 44.70%, respectively, with AC having a higher porosity value, and this demonstrates that AC particles are lighter than CP particles because AC particles have a porous structure, whereas CP particles have a denser and compact structure. The pores in the AC increase the surface area, which will be highly useful for the development of yeast biofilms when utilized as yeast MFC anodes. Meanwhile, Fig. 2a depicts the particle size distribution of CP and AC based on sieve analysis.

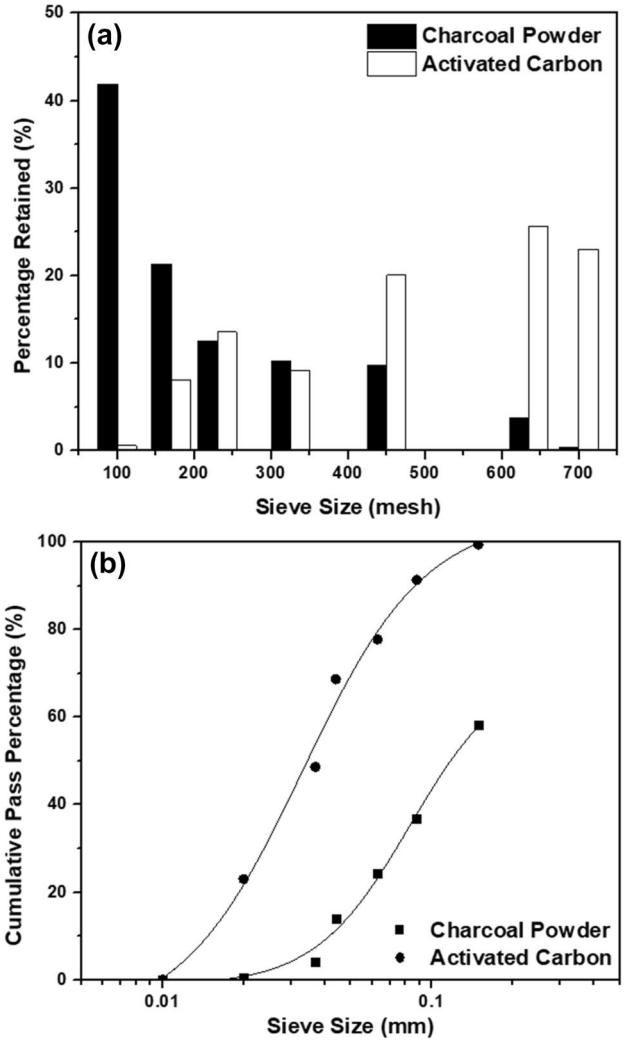

Fig. 2 **a** Particle distribution and **b** particle gradation diagram for AC and CP

Figure 2a shows that major AC particles (about 25.62%) retained in the 635-mesh sieve, while only 3.76% of CP particles retained in the same size mesh sieve and much more in 100 mesh (41.87%), showing that AC contains finer particles than CP. The smaller particle size makes it simpler to penetrate and distribute the CF. Then, the sieving analysis graph is presented in Fig. 2b, while the pH of AC and CP were 10.3 and 10.9, respectively.

3.2 Morphology analysis

In addition, CF that had been treated with CP or AC was evaluated for its physical. Based on the synthesis performed on CF, which has a projected surface area of 7 cm^2 and a thickness of 0.4 cm, the AC contained in CF was 33 mg cm^{-3}, which is 32% higher than CP, while the CP contained in CF is about 25 mg cm^{-3}. This is due to the

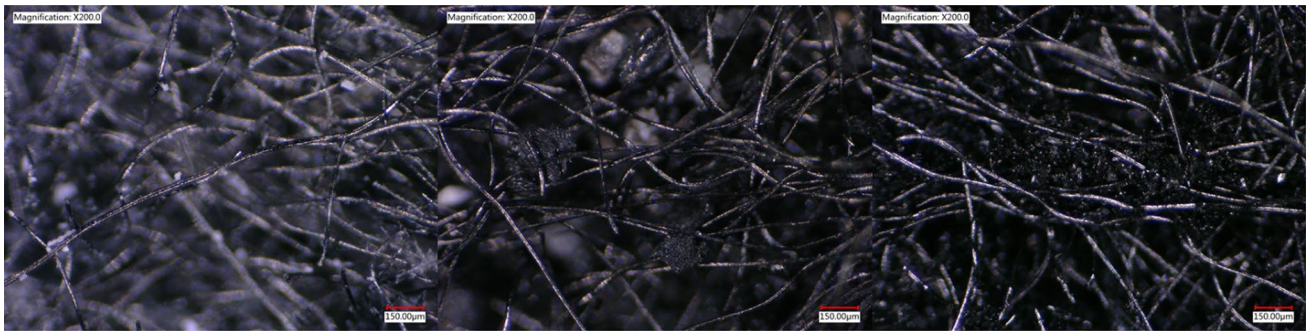

Fig. 3 DOM for CF (left), CF/CP (middle), and CF/AC (right) at 200 × magnification

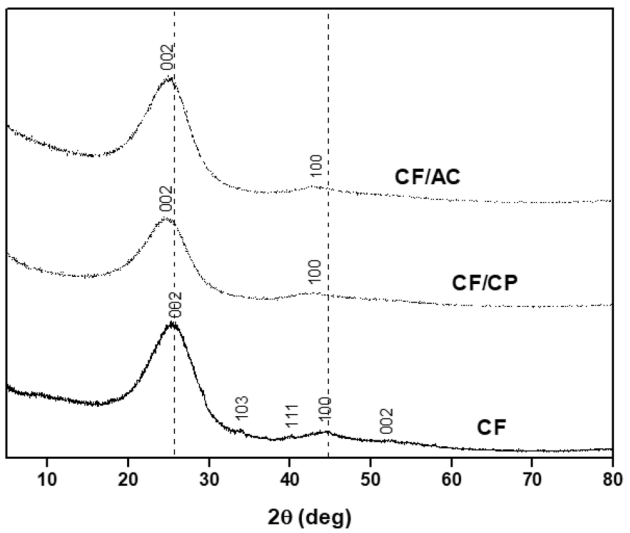

Fig. 4 XRD spectra of CF, CF/CP, and CF/AC anodes

smaller particle size of AC, which allows it to be easily distributed and penetrate into the CF, increasing the quantity contained in the CF. Morphological study using DOM was done for both CF, CF/CP, and CF/AC to confirm the bond between CF and AC or CP (Fig. 3). In CF, only fibers from single carbon felt are visible; however, in the CF/CP and CF/AC images, AC or CP may be seen between the CF fibers. The presence of drying following the modification process also aids in the binding of AC or CP to the CF, making them difficult to separate.

3.3 XRD analysis

XRD measurements were used to describe the crystalline morphology of the material of the CF electrode modified by CP or AC. Figure 4 shows the XRD patterns of CF, CF/CP, and CF/AC, respectively, where the two most noticeable diffraction peaks of 2θ occurred at 25° and 44°, as reported by precious related results [36, 37]. In addition,

Table 1 The lattice constants, unit cells volume, and crystallite size of CF, CF/CP, and CF/AC anodes

Anode structure	a = b (Å)	c (Å)	Volume of unit cells (Å^3)	Crystallite size (nm)
CF	2.25	7.03	35.59	1.03
CF/CP	2.12	7.31	32.85	1.18
CF/AC	2.08	7.18	31.06	1.48
JPCDS 00–041-1487	2.47	6.72	40.99	–

the 2θ = 25° and 44° peaks at CF/CP and CF/AC were discovered to shift slightly towards the smaller angle. This shift is probably affected by significant residual stress due to changes in the volume of the crystal during the reaction of CP or CP's deposition on CF. Furthermore, compression stress in the direction of measurement possibly contributes to a reduction in the lattice parameter, where the crystallite size increases as the peak angle reduces. Several peaks were also detected in CF diffraction at about 2θ = 34°, 40°, as well as 53°, and these are possibly due to remnants of CF impurities from the synthesis. However, these peaks were not observable for CF/CP and CF/CA, presumably because the impurities are lost during the CP and AC deposition on CF.

Once the XRD pattern is identified, the physical dimensions of the unit cells in the crystal lattice must be examined by finding the values of the lattice constants (a, b, c), using Eq. (5):

$$\frac{1}{d^2} = \frac{h^2 + k^2}{a^2} + \frac{l^2}{c^2}, \tag{5}$$

where h, k, and l represent the Miller indices (shown at each peak in Fig. 4), d represents the inter-planar spacing, while a, b, and c are the lattice constants of unit cells, where a and b are equal. Table 1 shows the lattice constants obtained for CF, CF/CP, and CF/AC, where the values of $a = b$ were 2.25, 2.08, and 2.12 Å, respectively, while the c values were

7.03, 7.18, and 7.31 Å, respectively. The lattice constants for the modified CF anode are somewhat similar to the lattice constants of graphite (JPCDS 00–041-1487), with the $a = b$ and c values of 2.47 Å and 6.72 Å, respectively. This indicates that graphite is the dominant building block of CF in the three modified CF anodes.

The crystallite size (D) must also be measured to prove the peak shift in the XRD diffraction curve. This measurement is carried out using Eq. (6), as shown in the following equation:

$$D = \frac{K \times \lambda}{C}, \tag{6}$$

where K is the shape factor (0.9), λ is the wavelength of X-ray source (1.5406 nm), C is the intercept of linear equation between 4sinθ and βcosθ, and β is the diffraction curve peak's Full-Width Half Maximum (FWHM). From these calculations, the crystal sizes of CF/AC were discovered to have the largest sizes of 1.48 nm, or 44% and 25% larger, compared to the CF/CP (1.03 nm) and CF (1.18 nm) counterparts, respectively. This is in line with the XRD findings, where the peak angles were discovered to reduce with an increase in crystal size. The relationship between crystallite size and electrical conductivity showed a reduction in the average crystallite size contributes to an increase in electrical conductivity [38]. Therefore, the CF anode presumable has better electrical conductivity, compared to the CF/CP or CF/AC counterparts. A study by Kumar et al., [39] reported that the larger the lattice constant or volume of unit cells implies, the smaller the crystal size, meaning that the two properties are inversely proportional.

3.4 Voltage and maximum power density of MFC

Figure 5a–c shows the MFCs with modified anode variance evaluated for power generation over three work cycle (144 h), with an external resistance of 1000 Ω. The MFC is then loaded with the fresh substrate, and the erratically varied voltage values recorded were attributed to the logarithmic phase of yeast, which makes attempts to adapt to the new environment [40]. In addition, there was a continuous increase in voltage values at about 24 h after the incubation time, followed by a period of stabilization. This outcome is attributed to the yeasts' logarithmic and stationary phases and the conditions to achieve the critical stage and initiate metabolism. Moreover, the effects recorded are possibly attributed to the electrochemically active biofilm formed on the anode surface. The modified anode material significantly affects the final voltage. The MFCs with CF/AC produce the highest voltage, with the stationary form ranging from 0.142 to 0.177 V, which is greater than the values recorded while using CF (range of 0.073 – 0.106 V) or CF/CP (0.088 – 0.131 V). Therefore, modifying CF with AC forms a 2D-3D electrode and greatly increases the bioelectric generation. The bifunctional role exhibited by the added material under this situation includes, first, those in tandem that provide a higher surface area, and is also beneficial for bacterial adhesion. The AC is characterized by more pores to promote adherence and yeast biofilm growth, being an active site compared to CP. Second, those used in conjunction with CF potentially improve the anode electrical conduction and effectively capture the electrons emitted from the yeast, before transferring to the CF.

Figure 5d–f shows the polarization curves calculated under the steady-state conditions of the MFC voltage. The modified anode material properties hugely influence the resulting power density (MPD). Specifically, those made with CF/AC anodes yield MPD measuring 54.58 ± 5.76 mW m^{-2}, or 442% and 142% beyond CF (10.07 ± 1.50 mW m^{-2}) and CF/CP (22.56 ± 0.26 mW m^{-2}), respectively. Furthermore, internal resistance was measured by adjusting the slope of the polarization curve [41]. The lowest internal resistance of 345 ± 87 Ω was reported in MFCs with a CF/AC anode, which is then the values recorded in those using CF (1478 ± 381 Ω) and CF/CP (714 ± 56 Ω). In addition, the use of AC modifies CF as 2D and 3D electrodes respectively form a 2D-3D hybrid. This substantially decreases the overall internal resistance during the incubation process and enhances the anode bioelectrochemical activity. Also, this modification process has instigated improvements in electron transfer efficiency from bacteria. Moreover, the large surface area of AC allows the bio-electrocatalytic process to ensue at sites inside the reformed anode with greater activity and consequently result in a higher power density.

Table 2 shows a comparison between the MPD values of several previous studies, and the yield of MFCs characterized by modified CF/AC anodes was equivalent or greater than any other work. The results obtained in prior research were approximately 5.1 – 1146 mW m^{-2}. Furthermore, this modification potentially increases the anode surface, allows for more biofilm growth on the surface, and increases the MFC output power. Therefore, the effects are observed for more stable electrochemical measurements. Table 2 also describes how MFC using *Geobacter* as a biocatalyst provides a higher power density compared to yeast or mixed consortia bacterium. *Geobacter* has nanowire parts that behave like artificial mediators, transferring ions generated in microbe cells to the electrode surface [42]. Furthermore, *Geobacter* has good metabolic activity, allowing it to transform fuel more effectively and efficiently into protons and electrons [43]. However, because yeast S. cerevisiae possesses the benefits described above, it is still worthy of consideration as an MFC biocatalyst.

The specific surface areas of CF, CF/CP, and CF/AC, determined based on calculations using Eq. (3) were 944,

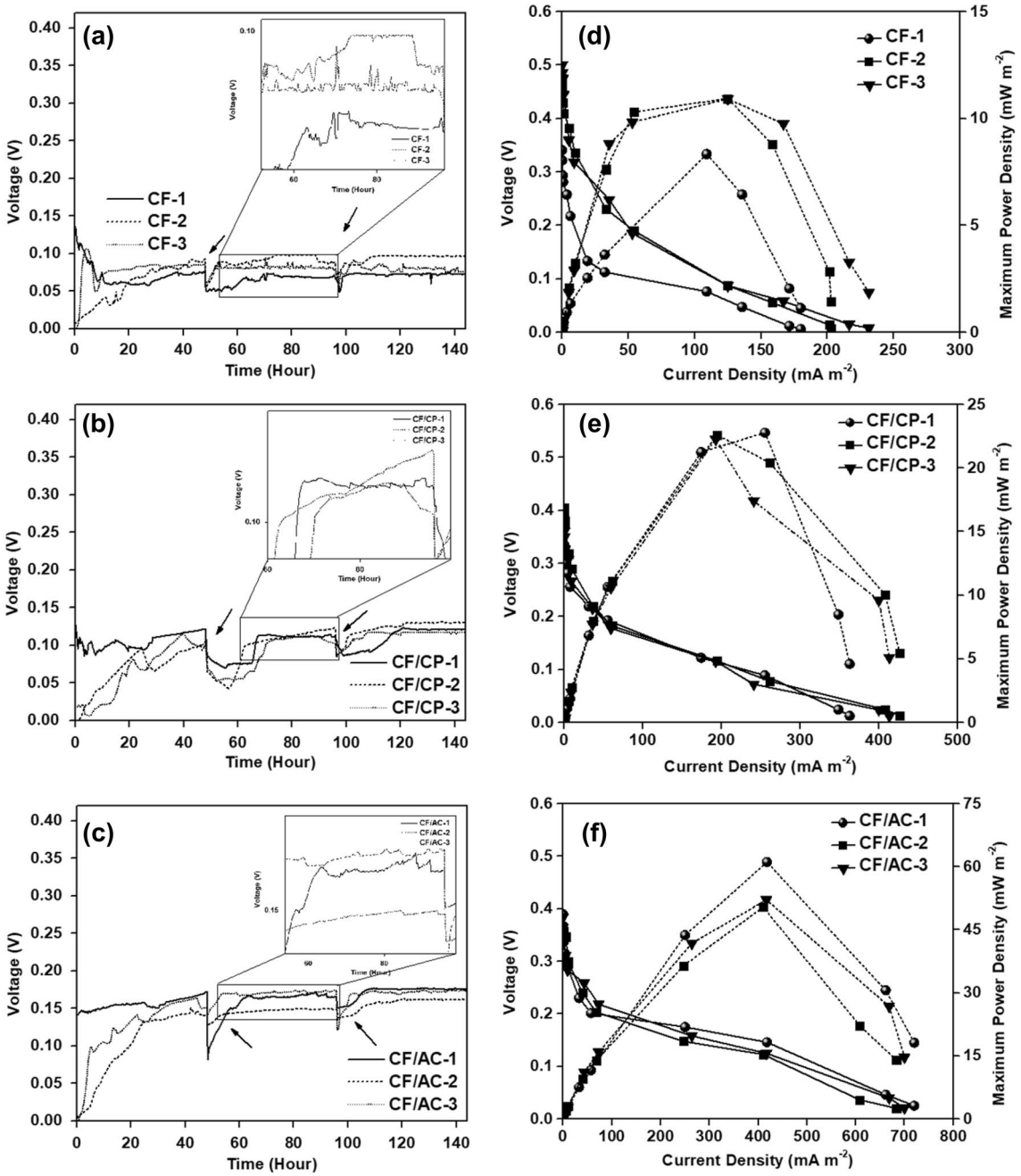

Fig. 5 Voltage produced during incubation process from MFC which used **a** CF, **b** CF/CP, and **c** CF/AC as their anode and **d–f** are their polarization curves, respectively. Inset shows the voltage stability in one cycle and arrows show the replacement time with fresh medium

996, and 1102 $m^2\ g^{-1}$, respectively. This clearly shows the capacity for AC or CP introduced to expand the electrode surface area of CF. Particularly, the AC-modified samples are possibly manufactured from cheap raw materials, through the easy method of electrodeposition immersion coating. These considerations make them popular candidates for the development of MFC with high performance.

3.5 Biofilm analysis

Figure 6 shows the anode SEM images after a 48 h incubation period. Picture 6a shows the yeast *S. cerevisiae* biofilm developed in the CF anode and not by AC or CP. Figure 6b and 6c are SEM images of CF, where *S. cerevisiae* yeasts used with modified CP and AC were dependent on biofilm growth. Figure 6a shows the well-developed biofilm

Table 2 The comparison MFC performance between this work and others

Anode structure	Biocatalyst	MPD (mW m^{-2})	References
activated carbon felt	*Escherichia coli*	38 (3.8 μW m^{-2})	[9]
Carbon cloth	*Shewanella* algae	50	[44]
graphite felt	Soil microbes	24	[45]
carbon paper	Mixed microbial consortia	5.1	[46]
carbon rods	Mixed microbial consortia	29.23	[47]
carbon felt	Mixed microbial consortia	45.4	[48]
carbon rod	*Geobacter sulfurreducens*	1146	[49]
graphite felt	*Geobacter* sp.	325	[50]
graphite rod	*Geobacter metallireducens*	396.7	[51]
CF/AC	*Saccharomyces cerevisiae*	54.58	This work

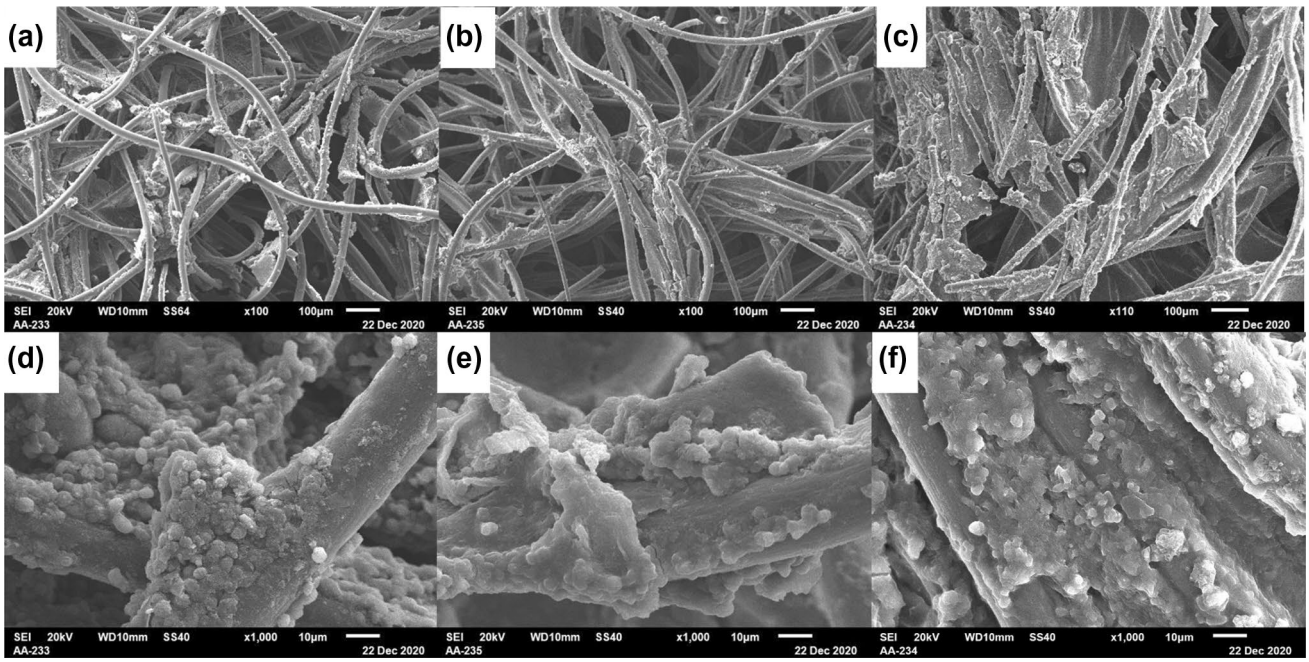

Fig. 6 SEM images of **a** CF, **b** CF/CP, and **c** CF/AC anode structure after an incubation process with 100 × of magnification, while **d–f** their SEM images, respectively, with a magnification of 1000×

developed on the CF material surface. This was also the case of CF/CP (Fig. 6b), although a more abundant consistency was observed. Figure 6c shows the high surface area in CF/AC, which resulted in excellent biofilm formation. Meanwhile, Fig. 6d-f shows the SEM images with higher magnification, where the biofilm adheres to the anode surface. The negatively charged yeast biofilm was attached due to the difference in charge [52, 53], and the effect of surface area on biofilm formation is seen. This figure also demonstrates the higher surface growth of CF/AC anodes in biofilm, with a considerably higher overall growth compared to CF or CF/CP. Therefore, the porosity in AC is critical for the success of the system, after deposition of CF in the available surface area. This experiment also shows evidence of very high yeast biofilm adhesion to AC/CF surface, leading to a relatively high surface area in the 2D-3D hybrid electrode. Therefore, the combination of material interconnection with the surface area accessed by biofilms is inferred to be construction sites with high significance in the development of productive anode materials.

Figure 7a shows the quantification of biofilm growth, which is conducted by performing the dry mass of the biofilm for each anode before and after the incubation process. The biofilm growth in CF/AC was approximately 0.043 ± 0.011 g, or 2.26 times higher than the values recorded for CF (0.019 ± 0.001 g) and 1.65 times higher than CF/CP (0.026 ± 0.001 g). This effect is attributed to changes in CF hydrophobicity, characterized by greater hydrophilicity. Therefore, exopolysaccharides (EPS) and lipopolysaccharides are considered to be very good materials for the

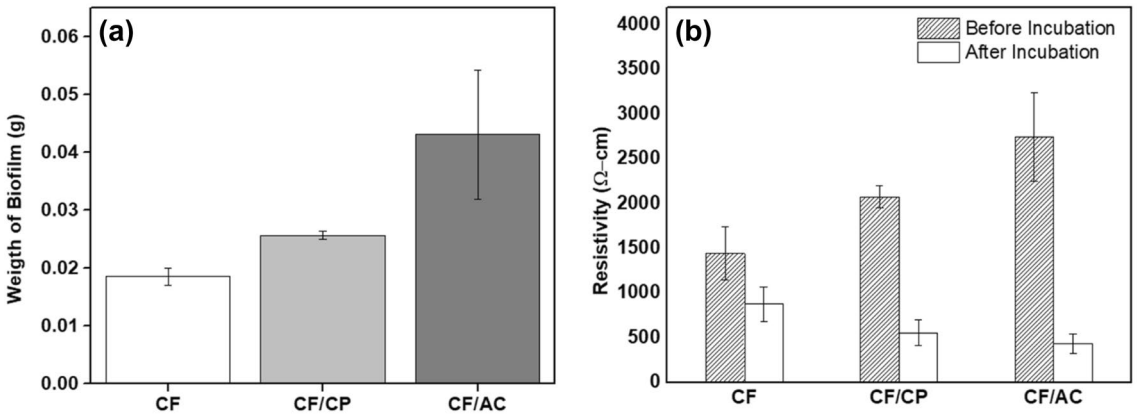

Fig. 7 **a** Weight of biofilm on the surface of CF, CF/CP, and CF/AC anode structure, while **b** is the resistivity of anode structures before and after the incubation process

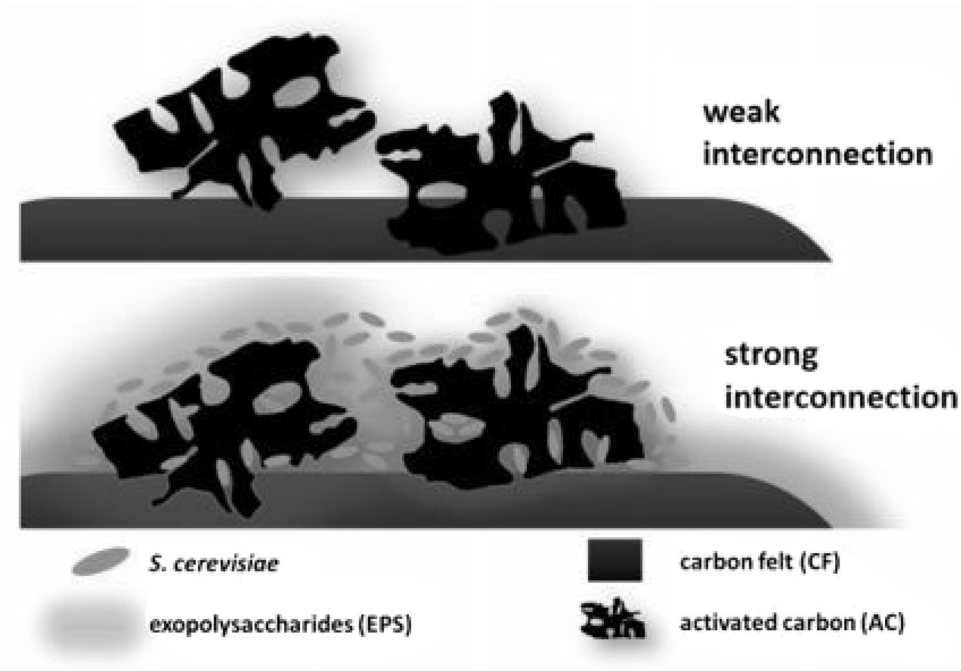

Fig. 8 Schematic of interconnection between CF, AC, and biofilm before and after incubation process

connection of biofilms with hydrophilic substances [54], and also in the promotion of biofilm growth on the anode surface. These results are consistent with the results of the above SEM images.

The CF electrode resistivity was tested to ascertain the efficacy of AC and CP deposition. Figure 7b shows the calculated resistivities for the CF, CF/CP, and CF/AC electrodes, indicating a higher resistance in the CF modified with AC or CP, and the highest values of about 2742 ± 495 Ω cm was reported in CF/AC, which was 90% and 32% higher than the outcome of CF (1444 ± 298 Ω cm) and CF/CP (2074 ± 125 Ω cm), respectively. This upsurge in resistance is possibly due to weak connections established during the deposition process between the carbon fibers in CF and CP or AC [9]. Also, it is important to recognize the inappropriateness of using binders as adhesive for the AC or CP deposition processes on CF. This finding correlates with the above XRD results, where CF showed the least resistivity and maximum conductivity. In addition, the anode resistance under steady-state conditions during the incubation period was also analyzed, and the calculation results identified the least values in CF/AC, at 433 ± 105 Ω cm, which is 51% lower than CF (876 ± 190 Ω cm) and 22% lower than CF/CP (557 ± 140 Ω cm). This small resistance value is attributed to the large number of yeast biofilms formed on the anode surface. The microorganisms show conductive properties, which are highly expressed in many electrodes, alongside a characteristic low resistance [55]. Furthermore,

Fig. 8 shows the interconnection between CF, AC, and biofilm both before and after the incubation process.

4 Conclusions

The power generation of an MFC is possibly improved by developing a 2D-3D electrode, through the combination of carbon felt (CF) as a 2D anode modified with activated carbon (AC) and charcoal powder (CP) as a 3D electrode. This results in a maximum power density of 54.58 ± 5.76 mW m^{-2}, which is 442% higher than CF at 10.07 ± 1.50 mW m^{-2}. The internal resistance of MFC with CF/AC anode was 51% smaller than the CF anode due to the huge quantity of biofilm on the surface. Furthermore, the combination of AC and CF offers numerous benefits to the overall performance, in terms of surface areas, good biocompatibility, and excellent electrical conductivity. These valuable properties encourage bacterial yeast growth, while the excellent electrical conductance encourages extracellular electron movement from the bacteria to the surface. This activity has led to a significant rise in MFC power generation, and the results are hoped to stimulate future interest in the architecture of hybrid 2D-3D anodes with high efficiency.

Acknowledgements This project was fully supported by the Hibah Penelitian Dasar 2021 given by the Indonesian Ministry of Education, Culture, Research and Technology (No. 163/E4.1/AK.04.PT/2021). The authors would like to thank Muhammad Rizky Adam Maulana and Sumaeroh from the Department of Chemical Engineering—Institut Teknologi Indonesia for their assistance in collecting data.

Declarations

Conflict of interest The authors declare that they do not have any conflicts of interest.

References

1. Kumar R, Singh L, Zularisam AW, Hai FI (2018) Microbial fuel cell is emerging as a versatile technology: a review on its possible applications, challenges and strategies to improve the performances. Int J Energy Res 42:369–394
2. Li T, Cai Y, Yang XL, Wu Y, Yang YL, Song HL (2020) Microbial fuel cell-membrane bioreactor integrated system for wastewater treatment and bioelectricity production: overview. J Environ Eng 146:04019092
3. Do MH, Ngo HH, Guo W, Chang SW, Nguyen DD, Liu Y, Kumar M (2020) Microbial fuel cell-based biosensor for online monitoring wastewater quality: a critical review. Sci Total Environ 712:e135612
4. Chen S, He G, Liu Q, Harnisch F, Zhou Y, Chen Y, Schröder U (2012) Layered corrugated electrode macrostructures boost microbial bioelectrocatalysis. Energy Environ Sci 5:9769–9772
5. Rinaldi A, Mecheri B, Garavaglia V, Licoccia S, Di Nardo P, Traversa E (2008) Engineering materials and biology to boost performance of microbial fuel cells: a critical review. Energy Environ Sci 1:417–429
6. Veerubhotla R, Das D, Pradhan D (2017) A flexible and disposable battery powered by bacteria using eyeliner coated paper electrodes. Biosens Bioelectron 94:464–470
7. Hashemi N, Lackore JM, Sharifi F, Goodrich PJ, Winchell ML, Hashemi N (2016) A paper-based microbial fuel cell operating under continuous flow condition. Technology 4:98–103
8. Feng J, Qian Y, Wang Z, Wang X, Xu S, Chen K, Ouyang P (2018) Enhancing the performance of Escherichia coli-inoculated microbial fuel cells by introduction of the phenazine-1-carboxylic acid pathway. J Biotechnol 275:1–6
9. Nguyen DT, Taguchi K (2019) Enhancing the performance of E. coli-powered MFCs by using porous 3D anodes based on coconut activated carbon. Biochem Eng J 151:e107357
10. Pomerantseva E, Bonaccorso F, Feng X, Cui Y, Gogotsi Y (2019) Energy storage: the future enabled by nanomaterials. Science 366:e6468
11. Sha J, Salvatierra RV, Dong P, Li Y, Lee SK, Wang T, Tour JM (2017) Three-dimensional rebar graphene. ACS Appl Mater Interfaces 9:7376–7384
12. Kholmanov IN, Magnuson CW, Piner R, Kim JY, Aliev AE, Tan C, Ruoff RS (2015) Optical, electrical, and electromechanical properties of hybrid graphene/carbon nanotube films. Adv Mater 27:3053–3059
13. Zhu S, Li J, Li Q, He C, Liu E, He F, Zhao N (2016) Space-confined synthesis of three-dimensional boron/nitrogen-doped carbon nanotubes/carbon nanosheets line-in-wall hybrids and their electrochemical energy storage applications. Electrochim Acta 212:621–629
14. Xiong P, Zhu J, Wang X (2015) Recent advances on multi-component hybrid nanostructures for electrochemical capacitors. J Power Sources 294:31–50
15. Zhou H, Zhang H, Zhao P, Yi B (2006) A comparative study of carbon felt and activated carbon based electrodes for sodium polysulfide/bromine redox flow battery. Electrochim Acta 51:6304–6312
16. Cheng S, Wu J (2013) Air-cathode preparation with activated carbon as catalyst, PTFE as binder and nickel foam as current collector for microbial fuel cells. Bioelectrochemistry 92:22–26
17. Liew KB, Daud WRW, Ghasemi M, Leong JX, Lim SS, Ismail M (2014) Non-Pt catalyst as oxygen reduction reaction in microbial fuel cells: a review. Int J Hydrogen Energy 39:4870–4883
18. Santoro C, Arbizzani C, Erable B, Ieropoulos I (2017) Microbial fuel cells: from fundamentals to applications. A review Journal of power sources 356:225–244
19. Smith RE, Davies TJ, Baynes NDB, Nichols RJ (2015) The electrochemical characterisation of graphite felts. J Electroanal Chem 747:29–38
20. Di Blasi A, Di Blasi O, Briguglio N, Aricò AS, Sebastián D, Lázaro MJ, Antonucci V (2013) Investigation of several graphite-based electrodes for vanadium redox flow cell. J Power Sources 227:15–23
21. Wang Y, Hasebe Y (2009) Carbon felt-based biocatalytic enzymatic flow-through detectors: chemical modification of tyrosinase onto amino-functionalized carbon felt using various coupling reagents. Talanta 79:1135–1141
22. Han L, Tricard S, Fang J, Zhao J, Shen W (2013) Prussian blue@platinum nanoparticles/graphite felt nanocomposite electrodes: application as hydrogen peroxide sensor. Biosens Bioelectron 43:120–124
23. Xiao L, Damien J, Luo J, Jang HD, Huang J, He Z (2012) Crumpled graphene particles for microbial fuel cell electrodes. J Power Sources 208:187–192
24. Shi J, Deng H, Lu L, Chen F, Xu H, Wang S, Xu F (2021) Performance of nickel–zinc battery with ZnO/activated carbon/3D

network carbon felt as zinc negative electrode. J Appl Electrochem 51:1675–1687
25. Shahzeydi A, Ghiaci M, Jameie L, Panjepour M (2019) Immobilization of N-doped carbon porous networks containing copper nanoparticles on carbon felt fibers for catalytic applications. Appl Surf Sci 485:194–203
26. Ganiyu SO, Le TXH, Bechelany M, Esposito G, van Hullebusch ED, Oturan MA, Cretin M (2017) A hierarchical CoFe-layered double hydroxide modified carbon-felt cathode for heterogeneous electro-Fenton process. J Mater Chem A 5:3655–3666
27. Shen Y, Wang W, Xiao K (2016) Synthesis of three-dimensional carbon felt supported TiO2 monoliths for photocatalytic degradation of methyl orange. J Environ Chem Eng 4:1259–1266
28. Zhang C, Liang P, Yang X, Jiang Y, Bian Y, Chen C, Huang X (2016) Binder-free graphene and manganese oxide coated carbon felt anode for high-performance microbial fuel cell. Biosens Bioelectron 81:32–38
29. Christwardana M, Frattini D, Duarte KD, Accardo G, Kwon Y (2019) Carbon felt molecular modification and biofilm augmentation via quorum sensing approach in yeast-based microbial fuel cells. Appl Energy 238:239–248
30. Christwardana M, Hadiyanto H, Motto SA, Sudarno S, Haryani K (2020) Performance evaluation of yeast-assisted microalgal microbial fuel cells on bioremediation of cafeteria wastewater for electricity generation and microalgae biomass production. Biomass Bioenerg 139:e105617
31. Christwardana M, Handayani AS, Yudianti R, Joelianingsih J (2021) Cellulose-Carrageenan coated carbon felt as potential anode structure for yeast microbial fuel cell. Int J Hydrogen Energy 46:6076–6086
32. Sayed ET, Barakat NA, Abdelkareem MA, Fouad H, Nakagawa N (2015) Yeast extract as an effective and safe mediator for the baker's-yeast-based microbial fuel cell. Ind Eng Chem Res 54:3116–3122
33. Tremaine JH, Miller JJ (1956) Effect of yeast extract, peptone, and certain nitrogen compounds on sporulation of Saccharomyces cerevisiae. Mycopathol Mycol Appl 7:241–250
34. Rouget G, Majidi B, Picard D, Gauvin G, Ziegler D, Mashreghi J, Alamdari H (2017) Electrical resistivity measurement of petroleum coke powder by means of four-probe method. Metall and Mater Trans B 48:2543–2550
35. Maltseva AA, Bibikova SB, Kalinichenko VN, Gudkov MV, Melnikov VP, Varfolomeeva SD (2018) Determining the specific surface area of carbon electrode materials for electrodes of supercapacitors via the adsorption of methylene blue dye. Russ J Phys Chem A 92:772–777
36. Banuelos JA, García-Rodríguez O, Rodríguez-Valadez FJ, Godínez LA (2015) Electrochemically prepared iron-modified activated carbon electrodes for their application in electro-Fenton and photoelectro-Fenton processes. J Electrochem Soc 162:E154
37. Fan W, Gao W, Zhang C, Tjiu WW, Pan J, Liu T (2012) Hybridization of graphene sheets and carbon-coated Fe 3 O 4 nanoparticles as a synergistic adsorbent of organic dyes. J Mater Chem 22:25108–25115
38. Šalkus T, Kazakevičius E, Banys J, Kranjčec M, Chomolyak AA, Neimet YY, Studenyak IP (2014) Influence of grain size effect on electrical properties of Cu6PS5I superionic ceramics. Solid State Ionics 262:597–600
39. Kumar D, Singh M, Singh AK (2018) Crystallite size effect on lattice strain and crystal structure of Ba1/4Sr3/4MnO3 layered perovskite manganite. AIP Conference Proceeding 1953:e030185
40. Christwardana M, Yoshi LA (2020) Performance and techno-economic analysis of scaling-up a single-chamber yeast microbial fuel cell as dissolved oxygen biosensor. Int J Renewable Energy Development 9:449–454
41. Logan BE (2008) Microbial fuel cells. John Wiley & Sons
42. Gorby YA, Yanina S, McLean JS, Rosso KM, Moyles D, Dohnalkova A, Fredrickson JK (2006) Electrically conductive bacterial nanowires produced by Shewanella oneidensis strain MR-1 and other microorganisms. Proc Natl Acad Sci 103:11358–11363
43. Bond DR, Lovley DR (2003) Electricity production by Geobacter sulfurreducens attached to electrodes. Appl Environ Microbiol 69:1548–1555
44. Choudhury P, Ray RN, Bandyopadhyay TK, Basak B, Muthuraj M, Bhunia B (2021) Process engineering for stable power recovery from dairy wastewater using microbial fuel cell. Int J Hydrogen Energy 46:3171–3182
45. Yu B, Feng L, He Y, Yang L, Xun Y (2021) Effects of anode materials on the performance and anode microbial community of soil microbial fuel cell. J Hazardous Mater 401:e123394
46. Sahu O (2019) Sustainable and clean treatment of industrial wastewater with microbial fuel cell. Results in Eng 4:e100053
47. Moharir PV, Tembhurkar AR (2018) Effect of recirculation on bioelectricity generation using microbial fuel cell with food waste leachate as substrate. Int J Hydrogen Energy 43:10061–10069
48. Shi J, Zhao W, Liu C, Jiang T, Ding H (2017) Enhanced performance for treatment of Cr (VI)-containing wastewater by microbial fuel cells with natural pyrrhotite-coated cathode. Water 9:979
49. Jiang Y, Song R, Cao L, Su Z, Ma Y, Liu Y (2019) Harvesting energy from cellulose through Geobacter sulfurreducens in unique ternary culture. Anal Chim Acta 1050:44–50
50. Kondaveeti S, Lee SH, Park HD, Min B (2020) Specific enrichment of different Geobacter sp. in anode biofilm by varying inter-spatial distance of electrodes in air-cathode microbial fuel cell (MFC). Electrochim Acta 331:e135388
51. Sindhuja M, Harinipriya S, Bala AC, Ray AK (2018) Environmentally available biowastes as substrate in microbial fuel cell for efficient chromium reduction. J Hazard Mater 355:197–205
52. Carlson G, Silverstein J (1998) Effect of molecular size and charge on biofilm sorption of organic matter. Water Res 32:1580–1592
53. Guo K, Soeriyadi AH, Patil SA, Prévoteau A, Freguia S, Gooding JJ, Rabaey K (2014) Surfactant treatment of carbon felt enhances anodic microbial electrocatalysis in bioelectrochemical systems. Electrochem Commun 39:1–4
54. Ramasamy RP, Ren Z, Mench MM, Regan JM (2008) Impact of initial biofilm growth on the anode impedance of microbial fuel cells. Biotechnol Bioeng 101:101–108
55. Hussain A, Lee J, Ren H, Lee HS (2021) Spatial distribution of biofilm conductivity in a Geobacter enriched anodic biofilm. Chem Eng J 404:e126544

Authors and Affiliations

Marcelinus Christwardana[1] · J. Joelianingsih[1] · Linda Aliffia Yoshi[1]

✉ Marcelinus Christwardana
marcelinus@iti.ac.id

✉ J. Joelianingsih
joelianingsih@iti.ac.id

[1] Department of Chemical Engineering, Institut Teknologi Indonesia, Jl. Raya Puspiptek Serpong, South Tangerang 15314, Indonesia